Available online at www.sciencedirect.com

ScienceDirect

Energy Procedia 1 (2009) 3453–3460

Energy Procedia

www.elsevier.com/locate/procedia

GHGT-9

Simplified Model for CO_2 Leakage and its Attenuation due to Geological Structures

Kyung Won Chang [a,b,*], Susan E. Minkoff [c], Steven L. Bryant [a]

[a] *Department of Petroleum and Geosystems Engineering, The University of Texas at Austin, Austin, TX 78712, USA*
[b] *Bureau of Economic Geology, Jackson School of Geology, The University of Texas at Austin, Austin, TX 78713, USA*
[c] *Department of Mathematics and Statistics, The University of Maryland, Baltimore County, Baltimore, MD 21250, USA*

Abstract

For risk associated with storage of CO_2 under the Earth's surface, the impervious cap is one of the most significant factors. Geological structures such as faults can provide conduits for CO_2 to escape through the cap. When conductive faults intersect the storage formation and overlying permeable layers, CO_2 leaks may exhibit three distinct behaviors: initial upward migration of fluids through the fault, lateral fluid movement through permeable layers, and continued movement of CO_2 along the fault above the leakage pathways.

To quantify this behavior, especially the attenuation, we develop a quasi-1D model for migration of buoyant fluid from a reservoir along a conductive fault. The fault can intersect multiple shallower formations. The model accounts for flow from the fault into a permeable formation using the concept of leakoff. The leakoff coefficient depends on the geometry and on the petrophysical properties of the formation. We use a commercial simulator (GEM from CMG) to run 2D verification studies of the 1D model. We present a series of examples that illustrate the controlling mechanisms for leakage rate from the reservoir and its attenuation by flux into shallower layers.

Leakage flux and its attenuation vary nonlinearly with the permeability of the fault and the permeability of the shallower layers intersected by the fault. Permeable layers near the CO_2 storage reservoir exhibit the greatest attenuation. While there is a nonlinear relationship between flux through the fault and the size of the leakoff coefficient, there is a linear relationship between the percentage which leaks off into neighboring formations and the ratio of fault permeability to leakoff coefficient. The rate of attenuation of CO_2 leakage depends on geometric and/or petrophysical properties of highly permeable structures as well as reservoir properties. An analytical derivation of the leak-off coefficient based on Darcy's equation compares favorably with 2D simulations. On the other hand, in the case of tilted permeable layers, calculation of the leakoff coefficient is less straightforward due to preferential flow within the layer (lighter CO_2 rising above heavier brine).

© 2009 Elsevier Ltd. All rights reserved.

Keywords: CO_2 sequestration; Leakage; Leakoff coefficient; Subsurface attenuation; Reservoir simulation; risk

* Corresponding author. Tel.: +1-512-232-5818; fax: +1-512-471-9605.
E-mail address: kyungwon.chang@gmail.com

doi:10.1016/j.egypro.2009.02.136

1. Introduction

In the standard approach to storage, CO_2 is captured from fixed sources such as coal-fired power plants, compressed and injected at supercritical conditions into a suitable target formation. An intact confining layer is necessary for several trapping mechanisms. However, sedimentary basins often contain geological discontinuities which are potential pathways for leakage through the confining layer. Faults are one such discontinuity and are prevalent in many regions where CO_2 storage is likely to be implemented.

It is therefore important to examine the consequences if injected CO_2 encounters a fault. A conductive fault can be a major pathway for the CO_2 plume due to its large transfer capacity. The rising CO_2 can be secondarily trapped by shallow subsurface structures, dissolution and residual phase creation (Lindeberg [1]). It can also migrate into permeable formations encountered by the conductive fault. On the one hand, this migration attenuates the upward flux. On the other, it spreads the influence of the CO_2 across a wider area. The near-surface zone can also attenuate CO_2 leaks and decrease CO_2 concentration reaching the surface. The attenuation rate is sensitive to the subsurface properties (Oldenburg and Unger [2]). Thus, the effect of a conductive fault on net CO_2 storage needs to be analyzed based on the geometric and petrophysical properties of the formation, of the fault, and of overlying permeable layer, and on the boundary conditions (pressure in the storage formation and in the overlying layers.)

Here we present a highly simplified model, motivated by geological and practical considerations. Leakage to the surface or to shallower permeable layers through the conductive fault will involve a sequence of upward (along a fault) and lateral (within a permeable layer) migrations. To reduce the uncertainty of physical properties of storage formations, simple models that allow adequate physics-based risk assessment will be valuable tools for operators, regulators and policymakers.

The model presented here was developed to be applicable within the Certification Framework (CF) for geologic storage (Oldenburg et al. [3,4]). One concept of the CF is that leakage occurs along conduits from the storage volume to "compartments" such as hydrocarbon reservoirs or underground sources of drinking water (USDW). The flux of CO_2 contributes to the risk associated with leakage. Thus the goal of the fault-leakage model is to estimate flux at an "outlet" of a conductive fault, once CO_2 has arrived at the "inlet." The sensitivity of the flux to physical parameters provides insight into which rock properties should be measured. This is important since deep saline aquifers provide large storage capacity but are not well characterized. Therefore, one goal of our fault-leakage model is to identify the key physical phenomena controlling leakage flux.

2. Modeling Approach

2.1. Assumptions & Description (Quasi-1D Model)

We assume that the CO_2 storage reservoir is located at sufficient depth for the carbon dioxide to be modeled as a slightly compressible fluid. If the CO_2 moves slowly enough to equilibrate with the pressure and temperature of the surrounding formations, slight compressibility is a reasonable assumption for both deep and shallow leaks. The pressure-temperature profile does not cross the gas/liquid phase boundary so that we need not treat phase transitions (Pruess [5]).

We treat the fault as a one-dimensional conduit. This means we average the complexities of the fault core and the damage zone surrounding it into a single array of permeability values. The relative displacement of sand bodies and shale layers along a fault causes the fault core to be very heterogeneous. Therefore, accounting for permeability variation along the fault will be important in estimating the risks associated with faults for a geologic storage project. The fault contains water initially (implemented by assuming the initial pressure along the fault is hydrostatic). The top of the fault is assumed to be at hydrostatic pressure. The bottom boundary of the fault is in contact with an over-pressured CO_2 source, the driving force for fluid migration up the fault. The value of this over-pressurization is proportional to the height of the column of stored CO_2 and the density difference between brine and CO_2. The pressure in the CO_2 phase is taken to be hydrostatic at the base of the column.

We further simplify the problem by assuming single-phase, Darcy flow within the fault. With these assumptions, the continuity equation becomes

$$\rho\phi c_t \frac{\partial p}{\partial t} = \frac{\partial}{\partial z}\frac{\rho k}{\mu}\left(\frac{\partial p}{\partial z} - \rho g \sin\theta\right) + q_{atten}$$

where θ is the inclination angle of the fault and q_{atten} represents the leakage into formations intersected by the fault.

The model is "quasi"-1D because CO_2 is allowed to enter neighboring strata lateral to the fault, but flow in these lateral formations is not explicitly modeled. Because we represent the fault as a "leaky conduit", we refer to flow into these strata as "leakage". The connotation of "leakage," that is, flow from the fault vs. flow from the storage formation, should be clear from the context. We model leakage from the fault via a specially designed source term. The lateral formations may be horizontal or inclined. The angle of inclination adds buoyancy to the driving force for leakage into the lateral formation.

2.2. Leakoff coefficients

The leakoff coefficient C in the source term can be estimated from the formation and fluid properties. This estimate is based on Darcy's law and the modeling assumptions described above. Assuming further that flow into the layer is steady, linear, and one-dimensional, we write

$$q(z) = \frac{k_r k_{layer}(z) A}{\mu} \frac{\Delta\Psi(z)}{L} \tag{1}$$

where q is volumetric flow rate of CO_2 at reservoir conditions, k_r is relative permeability, k_{layer} is absolute permeability of the layer into which CO_2 enters, A is cross-sectional area for leakage (i.e. the area of the intersection between fault and layer), L is the distance between fault and the far boundary of the layer, where the pressure is hydrostatic, and $\Delta\Psi$ is potential difference. The leakoff coefficient is obtained from writing Eq. (1) as a flux:

$$\Phi(z) = \rho(z) q(z) = C(z) \Delta\Psi(z) \tag{2}$$

where Φ is the mass flux into the layer and C is the leakoff coefficient, defined by

$$C(z) = -\frac{\rho(z) k_r k_{layer}(z)}{\mu(z) L} \tag{3}$$

The minus sign in Eq. 3 makes q a sink term in the continuity equation for flow in the fault. The leakoff coefficient consists of five parameters: CO_2 density and viscosity, relative permeability, absolute layer permeability, and distance from a fault to hydrostatic boundary. The absolute permeability of the layer differs in general from the fault permeability at the same depth. The relative permeability is evaluated at the CO_2 saturation at the Buckley-Leverett front. The frontal saturation is easily computed graphically from an extension of fractional flow theory that accounts for the mutual solubility of water and CO_2 (Noh *et al*. [6]). The distance L measures the extent of the pressure perturbation within the layer.

2.3. Assumptions & Descriptions (2D Model)

To test whether the 1D model is a reasonable physical approximation, we also carried out simulations of the full physics of the problem in 2D. Our 2D model is based on multi-phase flow of two fluids (CO_2 and brine) through a homogeneous and isothermal formation located at 1615 m (5300 ft) below the surface. Initially the target reservoir is fully saturated with CO_2 (S_g = 1.0) and is surrounded by an impermeable formation. Leakage occurs at the intersection with a conductive fault on the top seal of the CO_2 reservoir. The vertical conductive fault can be simulated using a large transmissibility multiplier (>> 1) on one specific column of grid blocks (Chang [7]). The storage formation is set at higher initial pressure (3.45 MPa or 500 psi more) than the surrounding formation to account for the larger pressure during CO_2 injection and for the smaller pressure gradient (5.61 kPa/m or 0.248 psi/ft) in the CO_2 column. Outside the storage reservoir, the pressure gradient is taken to be hydrostatic (9.79 kPa/m or 0.433 psi/ft). At side boundaries, constant pressure wells are placed to mimic a far-field constant pressure boundary. We also placed an injection well within the storage formation to replace CO_2 that escapes along the fault, thereby maintaining constant pressure within the storage formation (22.06 MPa or 3200 psi). Finally we place a constant-bottomhole-pressure production well (set to hydrostatic pressure) in the grid block at the top of the fault to mimic the open top boundary in the quasi-1D model. We use the GEM compositional simulator (Nghiem et al. [8]) to carry out this part of the study.

3. Results and Analysis

3.1. Quasi-1D Results

In these experiments we consider a 1000 m (3280 ft) long vertical fault located at a depth of 1000 m (3280 ft). We will assume in all of the experiments that follow that the CO_2 storage reservoir abuts the bottom of the fault and that the storage compartment is 500 m (1640 ft) thick, resulting in an over-pressurization of 5 MPa (725 psi) at the top of the reservoir (bottom of the fault). We use constant CO_2 viscosity of 0.00005 Pa-s, an initial reservoir porosity of 20%, an initial fluid pressure of 18 MPa (2611 psi), and an initial CO_2 density of 647 kg/m^3 (40.39 lb/ft^3). The rock compressibility is 1×10^{-11} Pa^{-1}, while the fluid compressibility value is 1×10^{-9} Pa^{-1}.

Our first conclusion is that leaks near the bottom of the fault have a greater impact than leaks which occur at shallower depths. Figure 1a shows the steady state mass flux along a fault when there are two lateral leakage pathways. Escaping from the storage formation is 0.26 kg CO_2/m^2-s. Most of this flux (about 80%) enters the deeper permeable formation at 1800 m (5900 ft). Relatively little attenuation (about 5% of the escape flux) occurs in the shallower permeable formation. Only 15% (0.07 kg CO_2/m^2-s) of the CO_2 escaping the storage formation reaches the top of the fault. Figure 1b shows that much less CO_2 leaves the storage formation when only the upper layer is present, but the attenuation is also much reduced. Consequently the flux escaping the top of the fault is actually larger than in Fig. 1a, even though the flux escaping the storage formation is smaller. This nonlinearity highlights the importance of accounting attenuation in risk assessment.

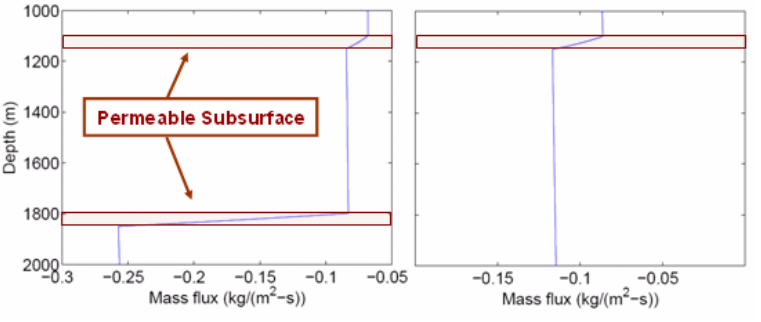

Fig 1. Quasi-1D model results for the effect of the location of permeable layers on CO_2 leakage and attenuation. The deeper the permeable layers are located, the more attenuation of CO_2 occurs. Hence a large flux escaping the storage formation need not imply a large flux escaping through the top of the fault.

The variation of permeability within the fault strongly affects leakage flux along the fault, especially when attenuation is possible. The results in Fig. 2 are for a fault intersecting one permeable formation between 1700 m and 1750 m. The fault has permeability 10^{-12} m^2 except at a "choke point", a low permeability ($k = 10^{-16}$ m^2) interval between 1400 m and 1500 m depth. The behavior depends on the leakoff coefficient for the permeable layer, which varies from -1.5×10^{-8} to -1.5×10^{-11} sec/m. Each figure compares the mass flux along the fault with constant fault permeability of 1 D (blue curve) and the mass flux when the fault zone contains the choke point (magenta curve). As the leakoff coefficient decreases, the gap between the constant and variable permeability fluxes widens. In all cases the choke point reduces flux escaping the top of the fault almost to zero. But large fluxes can still escape the storage formation if a permeable layer exists below the choke point. In these cases the attenuation of the leak is nearly 100%. Thus leakage layer permeability (or leakoff coefficient) and fault permeability distribution together dictate where leakage will occur.

3.2. Comparison of Quasi-1D and 2D Results

For both 1D and 2D models we compute mass flux along the fault and attenuation rate which indicates the amount of CO_2 which enters the permeable strata. Reservoir properties are summarized in Table 1. As Figure 3 shows the 1D and 2D results have the same trend of CO_2 plume behavior: (1) CO_2 leaks from initial storage, (2) CO_2 attenuation occurs into intersected permeable layers, and (3) flow continues up the fault past the leakage layer. We also confirm the intuitive expectation that the more permeable the layer, the greater the attenuation. However, the attenuation does not increase linearly with the permeability of the layer. The permeability of the layer into which leakage occurs has two opposing effects on risk: smaller permeability decreases the rate at which CO_2 escapes the storage formation but increases the rate at which it rises above the leakage layer.

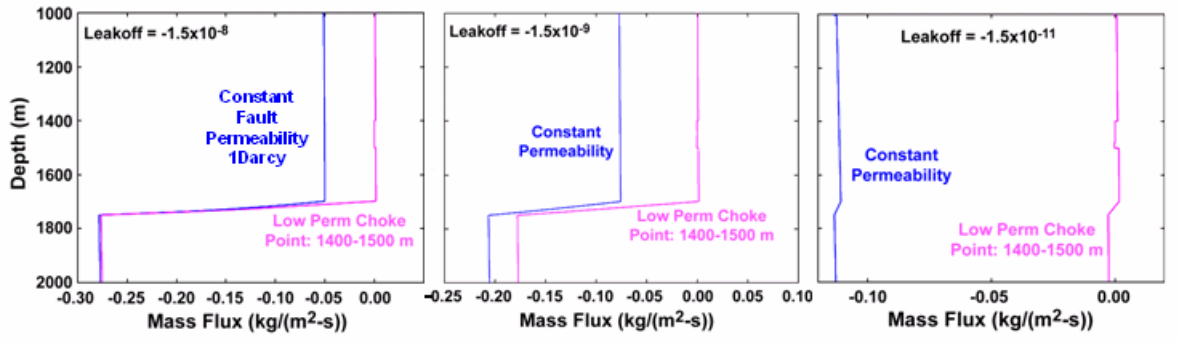

Fig 2. Comparison of leakage flux with a constant 1D permeability in the fault (blue) and with variable permeability in fault (magenta). The gap between the curves widens as the leak becomes smaller and the choke point above the leak becomes more significant.

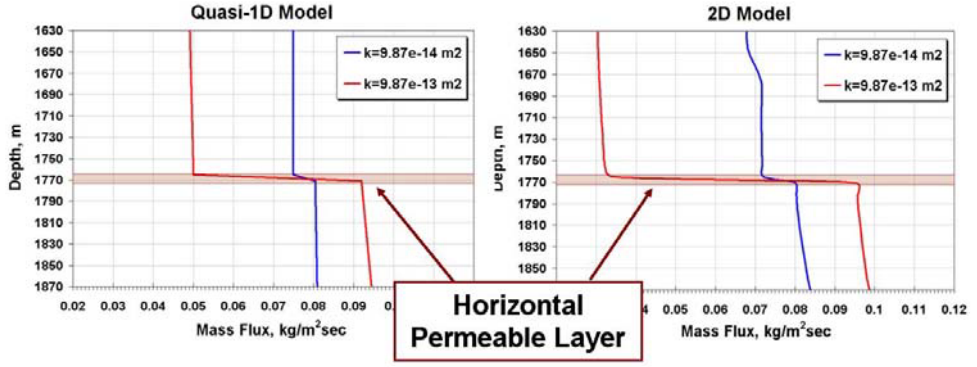

Fig 3. Mass flux distributions from quasi-1D model and from 2D full-physics simulation show similar trends. A fault ($k = 10^{-12}$ m^2) intersects a single permeable layer ($k_{layer} = 10^{-13}$ m^2 [blue] or $k_{layer} = 10^{-12}$ m^2 [red]). The leak is attenuated into the permeable layer. The more permeable the layer, the greater the flux escaping the formation, but the greater the attenuation; consequently less flux escapes the top of the fault.

The rates of CO_2 escape from the storage formation (leak flux in Table 2) are quite similar, but attenuation is less consistent between the models. The 2D model predicts larger attenuation rate and a weaker dependence of attenuation rate on layer permeability. A ten-fold reduction in layer permeability reduces attenuation by a factor of 6 in the 1D model and by a factor of 4.5 in the 2D model. We conclude that the 1D model captures the basic physics of the escape/attenuation process for short to moderately long faults. One qualification to this assertion is that the parameter L is well defined in the 2D simulation. For a fault intersecting an unbounded aquifer, a procedure to identify the appropriate value of L to enter into Eq. 3 needs to be developed.

3.3. Factors Controlling Leakoff Coefficient

3.3.1. Layer Properties (Permeability, Thickness & Dip Angle)

The layer permeability is one of the main factors which determines the attenuation rate of CO_2 flowing in a fault. Other geometric properties of the layer such as thickness (cross-sectional area) and dip angle should not influence leakoff coefficient. The result in Table 3 is consistent with our expectation from the definition in Eq. 3. Table 4 shows that the leakoff coefficient depends on dip angle. Tilting the layer by 14 degrees reduces the coefficient by a factor of two to three relative to the horizontal case. However, in the quasi-1D model the effect of dip angle should be accounted for in the potential difference term, $\Delta\Psi(z)$ in Eq. 2, and the leakoff coefficient should be independent of dip angle.

The reason for this discrepancy is that the dip results in countercurrent flow within the layer (see below). Only part of the layer accommodates CO_2 flux, while water moves in the remainder of the layer. Thus the leakoff coefficient could be correctly characterizing the conductivity of the layer for CO_2; the problem is for CO_2 movement,

the layer is in effect thinner than its nominal thickness. To account for this dip effect in the 1D model we could reduce the thickness of the interval where the leakoff coefficient is applied.

3.3.2. Rock Property (Relative Permeability Data)

Figure 4 shows the relative permeability curves and the corresponding fractional flow curves used to test sensitivity. The CO_2 phase endpoint relative permeabilities were changed, while the shape of the curves and the endpoint saturations were kept the same. Changing the drainage curve by a factor of three has only a slight effect on the observed leakoff coefficient (Table 5).

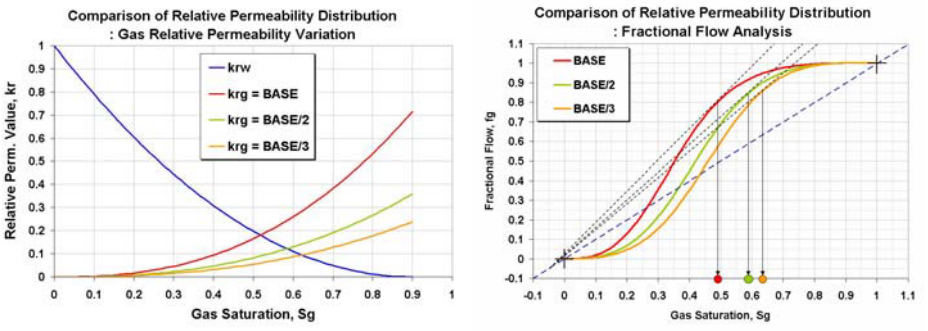

Fig 4. Artificially created relative permeability curves and their fractional flow curves; only drainage curves vary proportionally; Decreasing CO_2 phase saturation results in increasing its frontal saturation (Buckley-Leverett front). Then relative permeability of CO_2 plumes increases corresponding to given relative permeability curve

This result is counterintuitive, given the definition of C in Eq. 3. The explanation is that CO_2 establishes a front with a characteristic saturation as it rises, analogous to the Buckley-Leverett front saturation (Bryant *et al*. [9]). The value of the frontal saturation in turn determines the relative permeability characterizing the CO_2/brine displacement (Noh et al., 2007. Decreasing the CO_2 phase relative permeability increases this frontal saturation. Consequently, the relative permeability that is characteristic of the CO_2 leaking into the layer is larger. The competing effects cause the leakoff coefficient to be relatively insensitive to changes in the relative permeability.

3.4. Countercurrent Flow in Permeable Layer

The 2D full physics simulations show that less CO_2 enters a dipping layer than the 1D model predicts, but the models agree for horizontal layers. A grid refinement study reveals that countercurrent flow must accompany attenuation under these boundary conditions. The attenuated CO_2 mainly occupies the upper sub-layers of the permeable layer. Brine inside the permeable strata is displaced by CO_2 entering the strata. But brine also sinks (slowly) in the updip part of the layer, occupying the bottom sub-layer. Moreover the CO_2 extends a shorter distance in the downdip direction than updip. A larger dip angle amplifies these effects, hence the apparent leakoff coefficient inferred from the simulations decreases as dip angle increases (Table 6).

The modified leakoff coefficient obtained from these refined grid simulations is more consistent with analytical expectation, though some dependence on dip angle persists (Table 6). We remark that the 1D model is necessarily symmetric with regard to the leakage layer; it cannot account for different behavior in the downdip and updip sides of the layer.

4. Conclusion

We present a highly simplified version of carbon dioxide leakage along a fault which is suitable for incorporation in a risk assessment framework. The idealizations capture some of the essential physics and thereby provide insight on important couplings within the system. The model is an attempt to enable assessment of leakage fluxes when the flow properties of formations and faults intersecting them are poorly constrained.

The model assumes a 1D "leaky conduit" through which single phase, slightly compressible CO_2 flows. Leaks from the fault into permeable layer are modeled with a leakoff coefficient also based on Darcy's law. The leakoff coefficient depends on density and viscosity of CO_2, relative permeability, layer permeability, and the distance from attenuation point to hydrostatic boundary. Full-physics simulations in 2D indicate that this simple model is reasonable, and that the quasi-1D model captures key features of CO_2 migration in faults over moderate distances (< 1 km). The assumption of slight compressibility is the main limitation on applicability to longer distances.

The results from the quasi-1D model show that deeper layers provide much more attenuation than shallower layers. Ironically, more CO_2 escapes from the storage formation, but less CO_2 reaches the top of the fault, if the leakage layer is deeper. This nonlinearity is exacerbated if the fault has a low permeability section above the leakage layer. Thus attenuation can reduce risk associated with CO_2 reaching the top of the fault, even if more CO_2 leaves the storage formation. Attenuation is proportional to the ratio of fault permeability to leakoff coefficient. The interaction between CO_2 and water phases complicates attenuation behavior in the dipping layer. The denser fluid (brine) will occupy the lower part of a permeable zone depending on the dip angle. Consequently, applying the leakoff coefficient to the entire thickness of the layer will overestimate the attenuation.

Nomenclature

A	=	cross-sectional area of layer, ft^2 or m^2	q	=	flow rate of CO_2 at reservoir conditions, ft^3/sec or m^3/sec
C	=	leakoff coefficient, sec/ft or sec/m	z	=	depth, ft or m
c_j	=	compressibility, $j = f$ for fluid, $j = r$ for rock, psi^{-1} or Pa^{-1}	μ_{CO2}	=	viscosity of carbon dioxide, cp or Pa-s
k_{layer}	=	absolute permeability of layer, md or m^2	ρ_{CO2}	=	density of carbon dioxide, lb/ft^3 or kg/m^3
L	=	distance between fault and hydrostatic boundary, ft or m	Ψ	=	potential

Acknowledgements

The Geologic CO_2 Storage Joint Industry Project at The University of Texas at Austin supported this work. JIP members include BP, Chevron, CMG, ConocoPhillips, ExxonMobil, Landmark Graphics, Luminant and Shell.

References

1. Lindeberg, E., "Escape of CO_2 from aquifers," Energy Convers Manage. 38(Suppl.):S235-S240, 1997
2. Oldenburg, C.M. and Unger, A.J., "On Leakage and Seepage from Geologic Carbon Sequestration Sites: Unsaturated Zone Attenuation," Soil Science Society of America, Vadose Zone Journal, 2:287-296, 2003
3. Oldenburg, C.M., "Screening and Ranking Framework for Geologic CO_2 Storage Site Selection on the Basis of Health, Safety, and Environmental Risk," Environmental Geology; DOI 10.1007/s00254-007-0947-8, 2007
4. Oldenburg, C.M., Bryant, S.L., and Nicot, J.-P., "Certification framework based on effective trapping to meet the unprecedented challenges of geologic CO_2 storage (abs.)," *in* 2008 UIC Conference: What's hot in UIC!, Ground Water Protection Council, New Orleans, January 14-16, 2008
5. Pruess, K., "Numerical Simulation of CO_2 Leakage from a geologic Disposal Reservoir Including Transitions from Super- to Sub-critical Conditions, and Boiling for Liquid of CO_2," LBNL 52423, Lawrence Berkeley National Laboratory, 2003
6. Noh, M., Lake, L., Bryant, S.L. and Araque-Martinez, A., "Implications of Coupling Fractional Flow and Geochemistry for CO2 Injection in Aquifers," *SPEREE* **10** (4): 406-411. 2007
7. Chang, K., "A Simulation Study of CO_2 Migration in the Faulted Reservoir," Master Thesis, Univ. of Texas at Austin, 2007
8. Nghiem, L., Sammon, P., Grabenstetter, J. and Ohkuma, H., "Modeling CO_2 Storage in Aquifers with a Fully-coupled Geochemical EOS Compositional Simulator," SPE 89474 presented at SPE/DOE Improved Oil Recovery Symposium, Tulsa, OK, April 22-26, 2006
9. Bryant, S.L., Lakshminarasimhan, S., and Pope, G.A., "Buoyancy-Dominated Multiphase Flow and its Impact on Geological Sequestration of CO_2," SPE 99938 presented at SPE/DOE Improved Oil Recovery Symposium, Tulsa, OK, April 22-26, 2006

Table 1. Reservoir properties for quasi-1D and 2D models

Property		*Value*
Location	Fault	In the middle of reservoir
	Layer	5800 ft (below surface)
Perm.	Fault	9.87×10^{-13} m^2
	Layer	9.87×10^{-13} or 10^{-14} m^2
1D Leakoff Coeff.	1000 md Layer	5.24×10^{-9} sec/m
	100 md Layer	5.12×10^{-10} sec/m
Parameter for 2D Analytical Leakoff Coeff.	Rel. Perm. (k_r)	0.157
	Density (ρ_{CO2})	643.30 kg/m^3
	Viscosity (μ_{CO2})	6.81×10^{-5} Pa-s
	Distance (L)	304.8 m

Table 2. Comparison of CO_2 escape flux from storage formation and attenuation rate for quasi-1D and 2D models.

Layer Perm., m^2		*Leak Rate, kg/m^{2}s*	*Attenuation, %*
9.87×10^{-13}	1D	9.18×10^{-2}	46
	2D	10.00×10^{-2}	68
9.87×10^{-14}	1D	8.20×10^{-2}	8
	2D	8.49×10^{-2}	15

Table 3. Comparison of leakoff coefficients obtained from 2D simulations with different reservoir properties. Leakoff coefficients vary with absolute permeability of the layer, not with thickness, consistent with the definition in Eq. 3.

Layer Perm., m^2	*Layer Thickness, m*	*Leakoff Coeff. C, sec/m*
9.87×10^{-13}	3.05	5.24×10^{-9}
	9.14	4.92×10^{-9}
	15.24	4.95×10^{-9}
Analytical Solution		4.79×10^{-9}
9.87×10^{-14}	3.05	5.12×10^{-10}
	9.14	5.18×10^{-10}
	15.24	5.05×10^{-10}
Analytical Solution		4.79×10^{-10}

Table 4. Comparison of leakoff coefficient inferred from output of 2D simulations when layer dips. The dip should affect the driving force (Eq. 2) but not the leakoff coefficient (Eq. 3). However some variation of C is observed. The reason is that CO_2 does not occupy the entire thickness of the permeable layer.

Layer Perm, m^2	*Layer Geometry*		*Leakoff Coeff. C, sec/m*
9.87×10^{-13}	Horizontal		5.24×10^{-9}
	Tilted	Downdip	3.18×10^{-9}
		Updip	1.74×10^{-9}
9.87×10^{-14}	Horizontal		5.12×10^{-10}
	Tilted	Downdip	2.79×10^{-10}
		Updip	1.93×10^{-10}

Table 5. Comparison of leakoff coefficients; the variable parameter is relative permeability data. This table shows the leakoff coefficient is affected by relative permeability curve; decreasing the CO_2 phase relative permeability increases this frontal saturation. Consequently, the relative permeability that is characteristic of the CO_2 leaking into the layer is larger. The net result is that the leakoff coefficient is relatively insensitive to changes in the relative permeability.

Relative Perm.	*Layer Perm., m^2*	*Leakoff Coeff. C, sec/m*	
		Simulation	*Analytical*
BASE	9.87×10^{-13}	4.85×10^{-9}	4.79×10^{-9}
	9.87×10^{-14}	4.82×10^{-10}	4.79×10^{-10}
BASE2	9.87×10^{-13}	4.20×10^{-9}	3.74×10^{-9}
	9.87×10^{-14}	4.39×10^{-10}	3.74×10^{-10}
BASE3	9.87×10^{-13}	3.97×10^{-9}	3.05×10^{-9}
	9.87×10^{-14}	3.87×10^{-10}	3.05×10^{-10}

Table 6. Comparison of leakoff coefficient using refined grid blocks and analytical estimation.

Refined Grids System			*Leakoff Coefficient C sec/m*
Analytical Solution			2.39×10^{-9}
Simulation Horizontal Case			2.46×10^{-9}
Simulation Tilted Case	14°	Downdip	3.02×10^{-9}
		Updip	2.10×10^{-9}
	19°	Downdip	1.31×10^{-9}
		Updip	1.97×10^{-9}